Arteriosclerosis, Thrombosis, and Vascular Biology

BASIC SCIENCES

Calciprotein Particles Induce Endothelial Dysfunction by Impairing Endothelial Nitric Oxide Metabolism

Lian Feenstra, Anton G. Kutikhin, Daria K. Shishkova, Hendrik Buikema, Lara W. Zeper, Arno R. Bourgonje, Guido Krenning, Jan-Luuk Hillebrands

BACKGROUND: Calciprotein particles (CPPs) are associated with the development of vascular calcifications in chronic kidney disease. The role of endothelial cells (ECs) in this process is unknown. Here, we investigated the interaction of CPPs and ECs, thereby focusing on endothelial nitric oxide metabolism and oxidative stress.

METHODS: CPPs were generated in calcium- and phosphate-enriched medium. Human umbilical vein endothelial cells were exposed to different concentrations of CPPs (0–100 μg/mL) for 24 or 72 hours. Ex vivo porcine coronary artery rings were used to measure endothelial cell–dependent vascular smooth muscle cell relaxation after CPP exposure. Serum samples from an early chronic kidney disease cohort (n=245) were analyzed for calcification propensity (measure for CPP formation) and nitrate and nitrite levels (NO_x).

RESULTS: CPP exposure for 24 hours reduced eNOS (endothelial nitric oxide synthase) mRNA expression and decreased nitrite production, indicating reduced nitric oxide bioavailability. Also, 24-hour CPP exposure caused increased mitochondria-derived superoxide generation, together with nitrotyrosine protein residue formation. Long-term (72 hours) exposure of human umbilical vein endothelial cells to CPPs induced eNOS uncoupling and decreased eNOS protein expression, indicating further impairment of the nitric oxide pathway. The ex vivo porcine coronary artery model showed a significant reduction in endothelial-dependent vascular smooth muscle cell relaxation after CPP exposure. A negative association was observed between NO_x levels and calcification propensity ($r=-0.136$; $P=0.049$) in sera of (early) chronic kidney disease patients.

CONCLUSIONS: CPPs cause endothelial cell dysfunction by impairing nitric oxide metabolism and generating oxidative stress. Our findings provide new evidence for direct effects of CPPs on ECs and pathways involved.

GRAPHIC ABSTRACT: A graphic abstract is available for this article.

Key Words: calciprotein particles ■ chronic kidney disease ■ endothelial dysfunction ■ nitric oxide synthase type III ■ vascular calcification

Vascular calcifications (VCs) are a major cause of mortality and morbidity in patients with chronic kidney disease (CKD). Currently, the worldwide prevalence of CKD has been estimated around 13.4%, and between 47% and 92% of the CKD patients develop VC.[1–3] VCs in CKD are often the result of a decreased kidney function, which leads to disturbed mineral balances in the circulation.[4,5] Over the recent years, there has been an increasing interest in the formation of primary calciprotein particles (CPPs) as defense mechanism against hyperphosphatemia and hypercalcemia. Under physiological conditions, increasing phosphate and calcium levels are usually counteracted by the formation of primary CPPs, via the scavenging of free circulating calcium and phosphate by serum proteins such as Fetuin-A and albumin.[6–8] These initially formed primary CPPs are rapidly cleared from the blood via the liver and spleen.[9] However, in CKD, calcium and phosphate supersaturation, combined with the

Correspondence to: Jan-Luuk Hillebrands, PhD, Department of Pathology and Medical Biology, Division of Pathology, University Medical Center Groningen, University of Groningen, Hanzeplein 1 (EA10), 9713 GZ, Groningen, The Netherlands. Email j.l.hillebrands@umcg.nl
Supplemental Material is available at https://www.ahajournals.org/doi/suppl/10.1161/ATVBAHA.122.318420.
For Sources of Funding and Disclosures, see page 454.
© 2023 The Authors. *Arteriosclerosis, Thrombosis, and Vascular Biology* is published on behalf of the American Heart Association, Inc., by Wolters Kluwer Health, Inc. This is an open access article under the terms of the Creative Commons Attribution Non-Commercial-NoDerivs License, which permits use, distribution, and reproduction in any medium, provided that the original work is properly cited, the use is noncommercial, and no modifications or adaptations are made.
Arterioscler Thromb Vasc Biol is available at www.ahajournals.org/journal/atvb

Nonstandard Abbreviations and Acronyms

CKD	chronic kidney disease
CPP	calciprotein particle
EC	endothelial cell
eGFR	estimated glomerular filtration rate
eNOS	endothelial nitric oxide synthase
GC	guanylyl cyclase
NO	nitric oxide
RCA	right coronary artery
RUNX2	runt-related transcription factor 2
VSMC	vascular smooth muscle cell

Highlights

- In this study, we examine the effects of calciprotein particles (CPPs) on endothelial cell-functioning with the focus on the nitric oxide (NO) metabolism and oxidative stress.
- CPPs impair the endothelial cell–dependent relaxation of coronary artery rings ex vivo.
- CPPs decrease the NO bioavailability of endothelial cells (in vitro) via a reduction in endothelial nitric oxide synthase (eNOS) expression and function (eNOS uncoupling).
- Increased levels of superoxide radicals (O_2^-) are present in endothelial cells after CPP exposure.
- Clinical samples indicate a negative association between circulating nitrate/nitrite (NO_x) levels and calcification propensity (measure for CPP generation).

shortage of serum proteins and the reduced clearance of primary CPPs, results in the ripening of primary CPPs into the more harmful secondary CPPs.[6–8] Recently, accelerated formation of secondary CPPs (ie, increased serum calcification propensity) has been associated with the development of accelerated VC in CKD.[8,10,11]

A high calcification propensity, indicated by a shorter transition time (T_{50}) from primary to secondary CPPs, is associated with atherosclerotic vascular diseases and mortality in CKD patients (stage 2–4).[12] In addition, serum analysis of 200 CKD patients (stage 3–4) revealed that serum secondary CPP levels reflect a procalcific environment and can be linked to aortic stiffness.[13] When addressing the development of CPP-induced VC mechanistically, an important role for vascular smooth muscle cells (VSMCs) can be identified. Aghagolzadeh et al[14] demonstrated that secondary CPPs induce VSMC calcification in vitro via the activation of the TNF-α/TNFR1 pathway and the upregulation of oxidative stress. Additionally, CPPs isolated from CKD patients cause excessive mineral deposition and promote osteochondrogenic dedifferentiation of VSMCs in vitro.[15] Although the role of VSMCs in CPP-induced VC has been well established, the contribution of endothelial cells (ECs) to this pathophysiological process remains elusive. ECs form the inner layer of the blood vessels and are the first cell type interacting with circulating secondary CPPs.[16] This raises the question of whether secondary CPPs also affect EC-behavior and function.

ECs play an important role in the regulation of the vascular tone.[16] Various substances produced by ECs (including nitric oxide [NO]), endothelial-hyperpolarizing factors (eg, H_2O_2, CO, H_2S, and prostaglandins [PGI_2]) tightly balance and regulate vasodilation and vasoconstriction mediated by VSMCs.[17] NO is a gaseous compound that can be synthesized by nitric oxide synthases. Nitric oxide synthases are a family of 3 NO-generating enzymes (isoforms NOS 1–3), which all contribute to NO production. In ECs, eNOS (endothelial nitric oxide synthase/NOS3) is the predominant form and responsible for the largest part of NO production.[18,19] eNOS can be activated via the phosphorylation of the amino-acid residue Ser1177/Ser635, or via an increase in intracellular calcium.[18–20] Activation of eNOS leads to the conversion of O_2 and L-arginine to NO and L-citrulline. After synthesis, NO can diffuse from ECs to VSMCs, where it acts on the GC (guanylyl cyclase) pathway.[18–20] GC in VSMCs induces the formation of cyclic GMP, which decreases the intracellular calcium (Ca^{2+}) concentration via protein kinase G activation. The decrease of intracellular calcium reduces the actin-myosin cross bridge formation and results in VSMC relaxation.[18]

In conditions of cellular stress, the endothelial NO metabolism and NO bioavailability can be disturbed.[21,22] Various stressors like hyperglycemia and oxidized LDL particles can trigger the production of superoxides (O_2^-) via activation of NADPH-oxidases or mitochondrial O_2^- generation in ECs.[23–25] Additionally, superoxides can be generated via the uncoupling of eNOS.[26–28] In physiological conditions, eNOS functions in a dimer protein conformation. However, depletion of the L-arginine substrate or lack of cofactors like tetrahydrobiopterin (BH_4) can result in eNOS uncoupling, causing eNOS to function almost exclusively as monomer.[19] Although the primary effect of eNOS uncoupling is the reduced NO generation and bioavailability, an additional consequence is the production of superoxides via eNOS.[19,26–28] Increased superoxide generation in ECs can lead to the formation of peroxynitrite radicals ($ONOO^-$) via the reaction of O_2^- and freely available NO. Peroxynitrite radicals interact with lipids, DNA, enzymes and proteins and eventually affect multiple cellular processes and pathways.[29,30] Both the lack of NO bioavailability and a reduced eNOS functionality are considered as major contributors to EC dysfunction and the development of vascular diseases in CKD.[31,32]

In the present study, we investigate whether secondary CPPs affect the bioavailability of NO, and the NO metabolism of ECs, which may hamper EC function. To this end, we studied the impact of EC exposure to secondary CPPs in in vitro and ex vivo cell and tissue models, respectively and examined to what extent our preclinical findings could be translated to an early CKD patient cohort.

MATERIALS AND METHODS

Data supporting the findings in this study will be available upon reasonable request to the corresponding authors. The Supplemental Methods and the Major Resources Table can be found in the Supplemental Material.

Calciprotein Particle Generation

Ex Vivo Experiments

Calciprotein particles (CPPs) for ex vivo experiments were synthesized by the addition of 3.5 mmol/L phosphate (stock generated with 39% NaH_2PO_4 and 61% Na_2HPO_4) and 1 mmol/L calcium ($CaCl_2$) to Dulbecco's Modified Eagle Medium (DMEM 4.5*g*/L glucose and HEPES). The medium was supplemented with 10% non-heat inactivated FBS and 1% P/S and incubated for 14 days at 37 °C in the presence of 5% CO_2 (v/v). To collect the secondary CPPs after 14 days, the mixture was centrifuged once 30 minutes at 4000 rpm at RT and subsequently 30 minutes at 20 000×*g* at 4 °C with a table-top centrifuge.

In Vitro Experiments

CPPs for the in vitro experiments were synthesized by the addition of 3.5 mmol/L phosphate (NaH_2PO_4 exclusively) and 1 mmol/L calcium ($CaCl_2$) to Dulbecco's Modified Eagle Medium (DMEM 4.5*g*/L glucose and HEPES). The medium was supplemented with 10% non-heat inactivated FBS and 1% P/S and incubated for 14 days at 37 °C in the presence of 5% CO_2 (v/v). To collect the secondary CPPs after 14 days, the mixture was centrifuged twice for 2 hours at 24 000×*g* at 4 °C in an ultracentrifuge.

In between centrifugation steps, CPPs were washed with 1× TBS, after which the particles were reconstituted in 1x TBS. To measure CPP concentration, CPPs were solubilized for 3 hours in 0.6M HCl, and the concentration was evaluated by calcium content (µg/mL) measured with a Calcium Colorimetric Assay Kit (#MAK022, Sigma-Aldrich). Differences in CPP generation did not affect biological activity of the particles (eg, EC activation; data not shown). Maturity and crystallinity of the CPPs is validated with transmission electron microscopy and energy dispersive X-ray (EDX) analysis (Supplemental Methods and Figure S1).

Ex Vivo Tissue Samples

Porcine hearts were obtained from Kroon Vlees (Groningen, the Netherlands) within 30 minutes after sacrifice. To obtain the hearts, female pigs (≈75 kg) in the age of ≈7 months were sacrificed according to national procedures. Hearts were transported on ice in a buffered Krebs bicarbonate solution (NaCl, 120.4 mmol/L; KCl, 5.9 mmol/L; $CaCl_2$, 2.5 mmol/L; $MgCl_2$, 1.2 mmol/L; NaH_2PO_4, 1.2 mmol/L; glucose, 11.5 mmol/L; $NaHCO_3$, 25.0 mmol/L). To perform the ex vivo organ bath studies, the right coronary artery (RCA) was dissected in Krebs Buffer, cleaned of adhering fat tissue, and divided into individual rings (2–3 mm thickness).

Ex Vivo Organ Bath Studies

To assess the ex vivo endothelial cell function, RCA rings were incubated in Krebs-buffered CPP solutions (0=control condition, TBS in Krebs bicarbonate solution), 100, 200, and 400 µg/mL (CPPs) for 2 hours (37 °C) or overnight (≈20 hours, 4 °C). Rings were isolated from 3 individual porcine hearts and evenly distributed within groups (3–4 rings per heart per group; total 2 hours N=7–9 rings per group, overnight N=8–11 rings per group). After incubation, rings were placed into the organ baths for measurement of isotonic displacements as described previously.[33–35] In brief, organ baths were filled with Krebs buffer (15 mL) and continuously aerated with 95% O_2 and 5% CO_2 at 37 °C. Rings were allowed to equilibrate for 60 minutes before the start of the experiments. After the equilibrium was reached, rings were stimulated twice with 60 mmol/L KCl, for reasons of priming and viability assessment. Rings not responding to KCl treatment were excluded from the experiment. Then, rings were pre-contracted with the thromboxane agonist U46619 (10^{-7} mol/L) in the presence of the COX inhibitor indomethacin (10^{-5} mol/L). Because COX-derived prostaglandins can cause interspecies variation and thereby influence vasoactive responses, a single dose of indomethacin was administered to inhibit the prostaglandin activity and rule out COX-derived variation between pigs.[36] Subsequently, increasing concentrations of bradykinin (10^{-10}–10^{-6} mol/L) were added in a cumulative manner to measure endothelial-dependent relaxation of the rings. In this study, we used bradykinin as vasodilating compound, and not acetylcholine or H_2O_2 which are known to have vasoconstricting properties in various conditions.[37–39] To circumvent these vasoconstrictive effects, we chose to use bradykinin. Finally, a single dose of sodium nitroprusside (SNP; EC-independent NO donor; 10^{-4} mol/L) was added to assess maximal endothelium-independent VSMC relaxation. Both endothelial-dependent and endothelial-independent relaxation were calculated as percentage of the precontraction to U46619. Responses (in micrometer) were measured with LabView (National instruments, 2010). IC_{50} was calculated with GraphPad Prism 9.

Cell Culture

Human umbilical vein endothelial cells (HUVECs, Lonza) were cultured in endothelial cell medium (ECM; RPMI-1640 basal medium containing 20% FBS, 1% L-Glutamine, 1% P/S, 50 mg/L ECGF [homemade isolate according to Burgess et al[40]] and 5 U/mL heparin). Cells were expanded in T-75 flasks and sub cultured in T-25 culture flasks, 6 or 12-well plates, or Nunc Lab-Tek chamber slides (BD Biosciences), depending on the experimental purpose. All culture plastics were coated with 1% gelatin (porcine skin) solution in PBS (#G1890-100G, Sigma-Aldrich). Cells were kept at 37 °C (5% CO_2 (v/v)) and used between passage 4 and 6. For all in vitro experiments, HUVECs were stimulated with 0 (control condition, TBS in ECM), 50 and 100 µg/mL secondary CPPs for 24 or 72 hours.

Nitrite Assay

Nitrite is a stable breakdown product of bioactive NO and is often used as a marker for NO bioavailability and eNOS-NO output.[41] We approximated the NO levels using the Measure-iT™ High-sensitivity Nitrite Assay Kit (#M36051, Thermo Fisher Scientific). Hereto, Measure-iT™ quantitation reagent was combined with 10 µL of the quantitation standard solution or undiluted culture supernatant. After 10 minutes of incubation, Measure-iT ™ nitrite quantitation developer was added, and the absorbance was then measured in a plate reader using 365/450 nm excitation and emission wavelength. Nitrite levels were calculated with the standard curve after subtracting the background fluorescence. Data were expressed as the relative nitrite production normalized to the experimental control.

Gene Expression Analysis

RNA isolation was performed using TRIzol Reagent according to manufacturer's protocol. Purity and quantity of the extracted RNA were measured with the Nanodrop 1000 spectrophotometer (Thermo Fisher Scientific) and the ratios of absorbance at 260 and 280 nm ($A_{260/280}$) were consistently > 1.8. To synthesize cDNA, the cDNA reverse transcriptase kit (#4368813, Thermo Fisher Scientific) was used. Subsequently, RT-qPCR was performed using 5 ng of cDNA, SYBR Green PCR reaction mixture (Roche, Switzerland) and the following primer pairs: *eNOS* forward: AATCCTGTATGGCTCCGAGA and reverse: GGGACACCACGTCATACTCA, *β2M* forward: TTCTGGCCTGGAGGCTATC and reverse: TCAGGAAATTTGACTTTCCATTC. Analysis was performed in a 384-well plate on the LightCycler 480 system and software (Roche, Switzerland). Relative gene expression was calculated using the ΔC_T method. Data were presented as relative expression normalized to the experimental control.

Immunoblotting

Total protein was extracted from cells using RIPA buffer supplemented with a protease inhibitor (Sigma-Aldrich) and phosphatase inhibitor cocktail (Thermo Fisher Scientific). Protein concentrations were measured with a Protein Colorimetric Assay kit (#5000111, Bio-Rad). For gel electrophoresis, samples (20 µg) were loaded on 4% to 15% Mini-PROTEAN TGX Precast Protein Gels (#4561084, Bio-Rad). Immediately after running, samples were transferred on nitrocellulose membranes using the Trans-Blot Turbo RTA Mini Nitrocellulose Transfer kit (#1704270, Bio-Rad). Membranes were blocked in blocking buffer (5 g Elk Milk powder (Campina, the Netherlands) in TBS-1% Tween-20) for 1 hour at RT. After blocking, membranes were incubated overnight in TBS-1% Tween-20 with the primary antibodies specific for the phosphorylated eNOS (#612393, 1:500, BD Biosciences), total eNOS (#610296, 1:1000, BD Biosciences), GAPDH (#5174S, 1:1000, Cell Signaling Technology) and β-actin (#4967L, 1:1000, Cell Signaling Technology). Primary antibodies were detected using alkaline phosphatase (AP)-conjugated goat anti-mouse and goat anti-rabbit antibodies (#D0486 and #D0487, DAKO) or horseradish peroxidase (HRP)-conjugated rabbit anti-mouse and goat anti-rabbit antibodies (#P0260 and #P0448, DAKO). Blots were scanned with the HP-Scanjet 300 (HP, the Netherlands) or the ChemiDoc imaging system (Bio-Rad). Scans were analyzed with ImageJ Software[42] (National Institutes of Health) or ImageLab (Bio-Rad). Data were corrected for GAPDH or β-actin expression and presented as relative expression normalized to the experimental control. Relative phosphorylated eNOS expression was calculated by dividing the phosphorylated eNOS expression by the total eNOS expression.

eNOS Uncoupling

To determine the dimer/monomer protein ratio of eNOS, total protein was harvested from the cells using a Harvest Buffer (50 mmol/L Tris-HCL, 150 mmol/L NaCl and 0.5% Triton X-100).[43] Protein concentrations were measured with a protein colorimetric assay kit (#5000111, Bio-Rad). For the gel electrophoresis, samples were either boiled/denatured for 5 minutes at 95 °C followed by 10 minutes centrifugation at 14 000×*g* (to detect exclusively eNOS monomers) or maintained on ice (to detect intact eNOS dimers and monomers). Samples were loaded on 7.5% SDS gels for low-temperature SDS-PAGE. After gel electrophoresis, samples were transferred on nitrocellulose membranes using the Trans-Blot Turbo RTA Mini Nitrocellulose Transfer kit (#1704270, Bio-Rad). Membranes were scanned with the Gel Doc EZ imager (Bio-Radtotal protein input, and were then blocked in 3% BSA-PBS solution containing 1% Tween-20 for 2 hours at RT. To detect the eNOS protein, the blots were incubated overnight at 4 °C with the primary antibody for total eNOS (#610296, 1:1000, BD Biosciences). The secondary HRP-conjugated rabbit anti-mouse antibody (#P0260, DAKO) was used for the primary antibody detection. Finally, blots were scanned with the ChemiDoc imaging system (Bio-Rad) and have been analyzed with ImageLab (Bio-Rad). The uncoupling ratio of eNOS is determined by dividing the dimer by the monomer eNOS protein expression of the non-denatured sample. Total monomer expression in the boiled/denatured sample represents total eNOS expression. Data were corrected for the total protein input and presented as relative expression normalized to the experimental control.

Flow Cytometric Analysis

Flow cytometric analysis was used to measure superoxide (O_2^-) production in ECs. First, HUVECs were stimulated for 24 hours with CPPs, followed by 30 minutes incubation with 2.5 µmol/L MitoSOX Red Reagent (#M36008, Thermo Fisher Scientific). Next, cells were washed with serum-free ECM, detached with Trypsin-EDTA and centrifuged for 5 minutes at 300×*g* at RT. Thereafter, cells were resuspended in serum-free ECM (containing 180 nmol/L DAPI) and kept on ice until flow cytometry. The mean fluorescence intensity of DAPI-negative (viable) cells was quantified with the NovoCyte Quanteon-2 flow cytometer (Agilent Technologies). Graphs showed the geometric mean of the fluorescence intensity corrected for background fluorescence. Data were presented as relative expression normalized to the experimental control.

Fluorescent Imaging of Superoxide

To image superoxide (O_2^-) production, HUVECs exposed to secondary CPPs (24 hours) were incubated with 2.5 µmol/L MitoSOX Red Reagent (#M36008, Thermo Fisher Scientific), for 30 minutes at 37 °C. After incubation, cells were washed with serum-free ECM and fixed with 2% paraformaldehyde

(PFA) for 30 minutes. Prior to the imaging, samples were incubated with DAPI (180 nmol/L) solution for 10 minutes in the dark. Fluorescent images were taken with the EVOS cell imaging system (Thermo Fisher Scientific).

Nitrotyrosine Immunohistochemistry

To analyze peroxynitrite protein damage in ECs, indicated by the formation and presence of protein nitrotyrosine residues (3NT), an immunohistochemical nitrotyrosine staining was performed on HUVECs and paraffin-embedded RCA rings. With regard to the in vitro staining, HUVECs were cultured in Nunc Lab-Tek chamber slides (BD Biosciences) and exposed to secondary CPPs for 24 hours. After the stimulation, cells were fixed in 2% PFA and permeabilized with 0.5% Triton-X-100. Next, cells were blocked in 5% BSA-PBS and 0.1% H_2O_2 for 30 minutes at RT, followed by incubation with the primary anti-3NT antibody (#39B6, 1:50, Santa Cruz Biotechnologies) in 1% BSA-PBS at 4°C overnight. Cells were blocked with both avidin and biotin for 15 minutes at RT (#SP-2001, Avidin-biotin kit, Vector Laboratories). For detection of the primary antibody, an isotype-specific IgG_{2a} secondary antibody (#1081-08, 1:100, Southern Biotech, goat anti-mouse Biotin) and streptavidin-HRP conjugate diluted in 1% serum-PBS were used (#P039701-2, DAKO). Thereafter, tissue sections were incubated with 3'-diaminobenzidine (DAB) and counterstained with hematoxylin. Finally, stained HUVECs were mounted with Kaiser's glycerol gelatin. Stained sections were scanned with the Hamamatsu slide scanner (Hamamatsu, Japan) and analyzed with the ImageJ Software.[42] Graphs showed the mean pixel intensity expressed as delta (Δ) to the experimental control.

For staining the RCA rings, a similar protocol was followed with a few modifications. Briefly, the tissue sections were deparaffinized, followed by overnight antigen retrieval in 10 mmol/L Tris-HCl (pH=9) at 80°C. Tissue sections were blocked in 5% BSA-PBS and 0.1% H_2O_2 for 30 minutes at RT and incubated with the primary anti-3NT antibody (#39B6, 1:50, Santa Cruz Biotechnologies) in 1% BSA and 5% serum-PBS for 3 hours at RT. For the detection of the primary antibody, a donkey anti-mouse Alexa Fluor 647-conjugated secondary antibody (#A-31571, Invitrogen) was used. Additionally, tissue sections were incubated with *Lycopersicon esculentum* Lectin (LEA; #FL-1171, 1:100, Vector Laboratories) to visualize the endothelial glycocalyx. Nuclei were visualized with DAPI and sections were mounted with CitiFluor mounting medium. Stained sections were scanned the Olympus slide viewer VS200 (Olympus Nederland B.V., the Netherlands) and analyzed with the ImageJ Software afterward.[42] For analysis, 5 random LEA positive areas were selected, in which the mean fluorescent intensity of the 3NT positive pixels were quantified per sample.

Clinical Studies

Studies were approved by the Institutional Review Board of the Research Institute for Complex Issues of Cardiovascular Diseases (Kemerovo, Russia, protocol number #20180502, date of approval: 02 May 2018). Written informed consent was provided by all study participants. The investigation was conducted in accordance with the Good Clinical Practice and the Declaration of Helsinki. The study exclusively enrolled subjects with an estimated glomerular filtration rate (eGFR) >15 ml/min/m^2, mild to moderate CKD stages (1–3; n=245). A criterion of exclusion was missing data regardless of the reason. Data on age, sex and past medical history were collected at the time of admission. Peripheral blood samples were withdrawn into the BD Vacutainer polytetrafluoroethylene tubes with clot activator (#368815, BD) in the early morning the next day after the patients' admission. Serum has been obtained as soon as possible by means of blood centrifugation at 3000×*g* for 10 minutes and was subsequently transferred on ice to either clinical biochemistry laboratory (for the analysis of total and ionised calcium (Ca^{2+}), phosphate, total protein, albumin, and fetuin-A) or clinical pathophysiology laboratory (for the measurements of nitrates/nitrites, serum calcification propensity, and flow cytometry quantification of CPPs). Serum concentrations of total calcium, ionized calcium (Ca^{2+}), phosphate, total protein, and albumin were measured utilizing an automated biochemical analyzer (Konelab 60i, Thermo Fisher Scientific) and Fetuin-A levels were determined by an enzyme-linked immunosorbent assay (#RD191037100, BioVendor, Germany) according to the manufacturer's protocol. Levels of serum nitrates and nitrites (NO_x) were measured using a colorimetric Nitric Oxide Assay kit (#ab65328, Abcam, UK). NO_x is a biomarker of NO in clinical studies, as it represents the sum of the breakdown products of NO, nitrate (NO_3^-) and nitrite (NO_2^-).[44]

To measure serum calcification propensity (OD_{650}), equimolar (2 mmol/L) concentrations of $CaCl_2$ and Na_2HPO_4 were added to the serum of the subjects in 96-well plates (100 µL serum per well). Upon 24 hours incubation at 37°C in the presence of 5% CO_2 (v/v), the change in the optical density at a 650 nm wavelength (OD_{650}) was monitored by comparing the serum with or without calcium/phosphate supplementation. Relative quantification of CPPs in the serum was performed by the OsteoSense 680EX/PKH67 flow cytometric assay as described before.[45] Briefly, thawed serum was centrifuged at 3500 rpm for 5 minutes (RT) to sediment the cryoprecipitate. Then, 50 µL serum was added to 200 µL sterile-filtered Tris-buffered saline (pH 7.4) and centrifuged at 10 000×*g* for 15 minutes at 4°C to sediment the debris. The mixture (200 µL) was blended with 250 µL OsteoSense 680EX (#NEV10020EX, PerkinElmer, concentration 0.3 µmol/L) and incubated in the dark for 50 minutes at 4°C. Subsequently, 25 µL of PKH67 (#MINI67, Sigma-Aldrich, concentration 10 µmol/L) was added and the mixture was incubated in the dark for an additional 10 minutes at 4°C. The OsteoSense 680EX signal was detected using a 638 nm laser and 712/25 nm bandpass filter, while the PKH67 signal was measured with a 488 nm laser and 525/40 nm bandpass filter on the CytoFLEX flow cytometer (Beckman Coulter). For quantification of the CPP count, OsteoSense 680EX positive—PKH67 negative events were quantified, as OsteoSense 680EX binds CPPs and PKH67 discriminated the CPPs from similar-sized extracellular vesicles.

Statistical Analysis

Experimental data were analyzed with GraphPad Prism 9 (GraphPad software, CA) and presented as mean±SEM. Repeated measurements of the RCA ex vivo vascular function were analyzed using a 2-way repeated measurements ANOVA and Dunnett post-hoc test for multiple comparisons. Group differences were tested with 1-way ANOVA followed by a Dunnett or Tukey post-hoc test for multiple comparisons. Clinical data were presented as mean±SD, median with interquartile range

(IQR) or as proportions *n* with corresponding percentages (%). Normality assessment was performed by visual inspection of histograms and normal probability (Q-Q) plots. Subjects were divided into tertiles of calcification propensity (OD_{650}), followed by a comparison of population characteristics. Differences across tertiles were tested using 1-way ANOVA, Kruskal-Wallis tests or χ^2 tests, with a Bonferroni post-hoc test for multiple comparison. Univariable linear regression analyses were performed to study the associations between OD_{650} and NO_x levels and renal function (eGFR). From linear regression analyses, unstandardized beta-coefficients were reported with 95% CIs and corresponding *P*. Multivariable linear regression analyses (method: forced entry) were performed to allow adjustment for relevant covariates. Prior to analysis, OD_{650} and NO_x values were standardized using *Z*-scores (to facilitate comparison of predictor estimates) and eGFR as dependent variable was square-transformed in order to avoid violation of the normality and homoscedasticity assumptions. All model estimates were presented after back-transformation, meaning that unstandardized beta-coefficients represented the difference in eGFR per 1-SD increment or decrement in OD_{650} or NO_x. Assumptions of normality of residual variance and homoscedasticity for linear regression analysis were fulfilled. Clinical data were analyzed using SPSS Statistics software (v.25.0, SPSS Inc., Chicago, IL) and visualized using the *pandas* (v.1.2.3), *seaborn* (v.0.11.1.) and *matplotlib* (v.3.4.1) packages of the Python programming language (v.3.9.0., Python Software Foundation, https://www.python.org). For all statistical tests, 2-tailed $P<0.05$ were considered as statistically significant.

RESULTS

Overnight Exposure to Secondary CPPs Dose-Dependently Impairs Endothelial-Dependent Vasorelaxation

We first assessed whether secondary CPPs affect the endothelial-dependent vasorelaxation, using an ex vivo porcine coronary artery ring (RCA-ring) model. Whereas short-term (acute) exposure (2 hours) of secondary CPPs to the RCA-rings did not affect the endothelial-dependent vasorelaxation (Figure 1A), long-term (overnight) exposure showed a dose-dependent reduction in bradykinin-induced relaxation (Figure 1B). This decrease in dilation response was most abundant in the RCA-rings stimulated with 200 and 400 µg/mL of secondary CPPs (at bradykinin concentrations of 10^{-8}–10^{-6} M) compared with the control condition. The half-maximal inhibitor concentration (IC_{50}) did not significantly differ between the groups (Table S1). Presence of ECs in the RCA-rings after CPP exposure was validated with a CD31 staining (Supplemental Methods and Figure S2). Exposure of porcine arteries to various concentrations of CPPs did not result in massive denudation and loss of ECs, since the CD31 staining was preserved. However, staining intensity of CD31 appeared to be reduced at higher CPP concentrations, which might reflect EC-dysfunction.[46] Additionally, no direct effects of CPPs on VSMC function were found (responses to SNP, KCl and U46619; Figure S3).

Secondary CPPs Decrease the NO Bioavailability in Endothelial Cells

As the endothelial-dependent relaxation of the VSMCs was impaired in the RCA-rings after CPP exposure, we next determined whether the NO metabolism of the ECs is affected by CPPs as well. HUVECs stimulated with secondary CPPs (50 and 100 µg/mL) for 24 hours showed a reduced nitrite production (Figure 2A). Considering the nitrite production as an approximate of the eNOS NO-output, these results indicate a reduced NO bioavailability in ECs after CPP exposure. Additionally, eNOS mRNA expression tend to decrease after 24-hour exposure with secondary CPPs to HUVECs (Figure 2B). However, this decrease was only significant in HUVECs exposed to 100 µg/mL secondary CPPs. While eNOS total protein expression and phosphorylation (activation site Ser1177) remained unaltered after 24 hours of CPP exposure (Figure 2C through 2E), increasing the

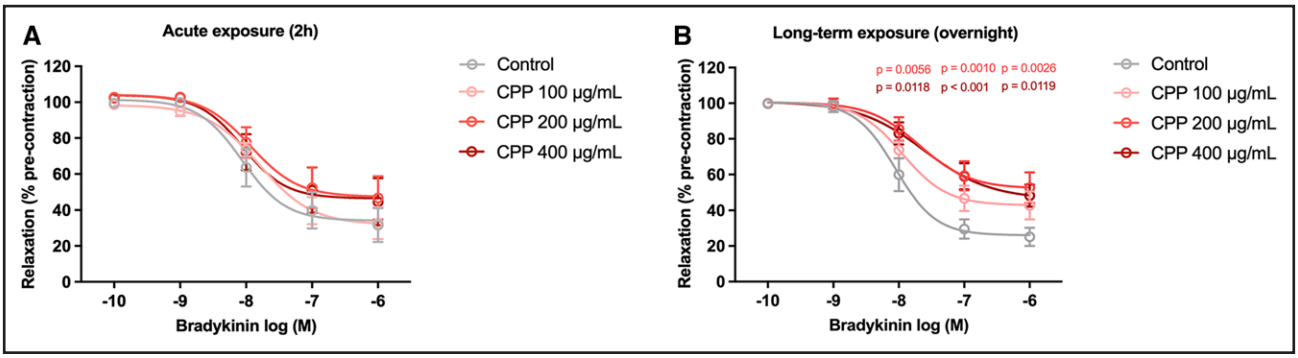

Figure 1. Reduced endothelial-dependent vasorelaxation in right coronary artery (RCA)-rings after secondary calciprotein particle (CPP) exposure.
A, Acute exposure (2 hours) of RCA-rings to secondary CPPs (control=0, 100, 200, and 400 µg/mL) did not affect the dilation response. **B**, Long-term exposure (overnight) of RCA-rings to secondary CPPs (CPP 200 µg/mL and 400 µg/mL) showed a significant reduction in endothelial-dependent vasorelaxation. Rings were isolated from 3 individual porcine hearts and evenly distributed within groups (3–4 rings per heart per group; total 2h N=7–9 rings per group, overnight N=8–11 rings per group). Data are shown as relaxation in % of precontraction to U46619. Graphs show means±SEM. Significant differences are indicated for $P<0.05$.

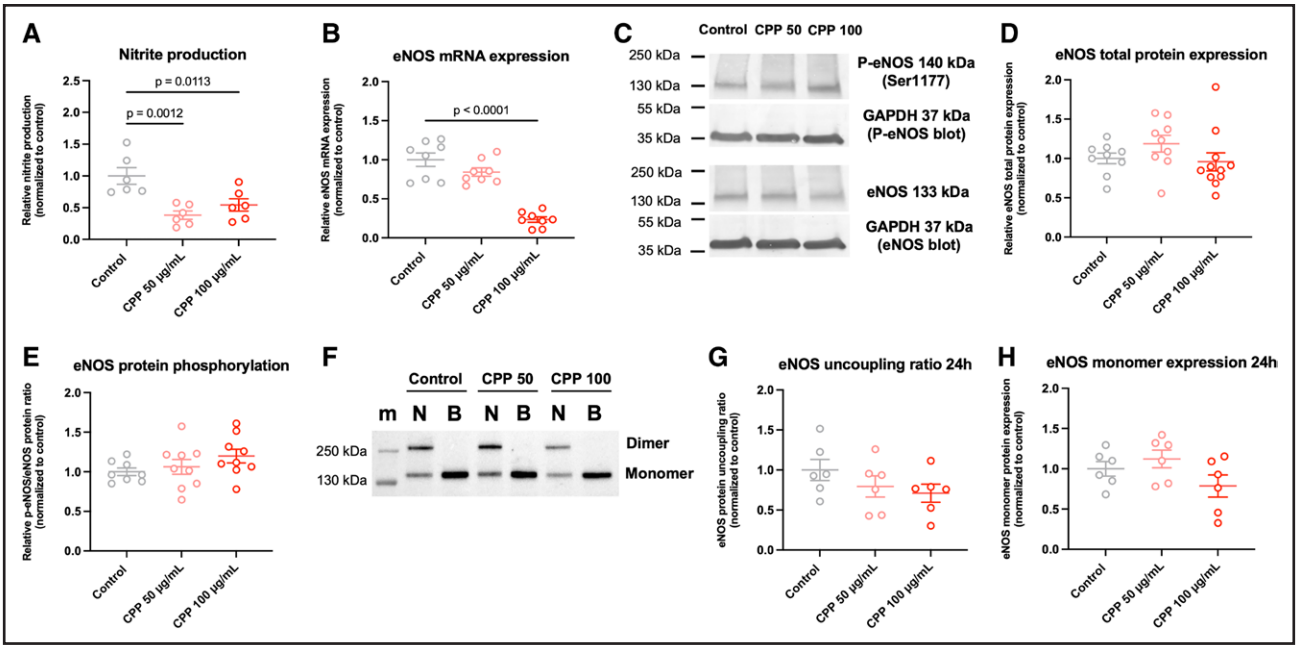

Figure 2. Exposure of secondary calciprotein particles (CPPs) to human umbilical vein endothelial cells (HUVECs) for 24 hours reduces NO bioavailability and eNOS (endothelial nitric oxide synthase) mRNA expression.
A, Nitrite production decreased significantly in HUVECs exposed to both 50 and 100 µg/mL secondary CPPs. **B**, eNOS mRNA expression was only significantly reduced after 24 hours of exposure to 100 µg/mL secondary CPPs. **C**, Representative protein blots showing phospho-eNOS (Ser1177), total eNOS and GAPDH (of both the P-eNOS and total eNOS blots). Molecular weight standards are indicated on the left side of the immunoblots in kilodaltons (kDa) based on the marker shown in Figure S7A and S7B. **D** and **E**, eNOS total protein expression and eNOS protein phosphorylation (Ser1177-activation site) were not affected in HUVECs after 24 hours of secondary CPP exposure. **F**, Low-temperature SDS-PAGE blots showing non-boiled/intact (indicated by symbol N) dimer/monomer eNOS expression, and boiled/denatured (indicated by symbol B) eNOS total monomer expression. Molecular weight standards of the marker (m) are indicated on the left side of the immunoblots in kilodaltons (kDa). **G** and **H**, eNOS uncoupling ratios (dimer/monomer ratio) and total eNOS monomer expression were not affected after 24-hour secondary CPP exposure to HUVECs. Data are presented as means±SEM with individual data points and normalized to the experimental control. Significant differences are indicated for $P<0.05$.

exposure time to 72 hours significantly decreased the eNOS total protein expression in ECs and increased the eNOS phosphorylation as compared with the 24-hour timepoint (Figure S4A through S4C).

Further, we examined eNOS uncoupling in ECs exposed to CPPs. By performing a low-temperature SDS-PAGE, both the monomer and dimer fraction of eNOS were determined. Data on HUVECs indicated a trend towards eNOS uncoupling (decreased dimer/monomer ratio) after 24-hour exposure of HUVECs to secondary CPPs (Figure 2F and 2G). Results were independent of an altered eNOS monomer expression (Figure 2H), which is in accordance with Figure 2D. When the exposure time was increased to 72 hours, the dimer/monomer ratio of eNOS reduced, indicating further eNOS uncoupling (Figure S4D and S4E). eNOS monomer expression was reduced as well (Figure S4D and S4F), confirming the observations indicated in Figure 4B.

Oxidative Stress and Peroxynitrite Radical Formation in Endothelial Cells

To evaluate whether secondary CPPs induce superoxide (O_2^-) formation in ECs, HUVECs exposed to secondary CPPs were measured for superoxide levels using the MitoSOX Red reagent. Flow cytometric analyses showed an increase in fluorescence intensity for HUVECs exposed to 100 µg/mL of secondary CPPs, compared with the human umbilical vein endothelial cell control (Figure 3A and 3B). Similar observations were made when visualizing MitoSOX Red with fluorescent microscopy (Figure 3C). These data indicate that secondary CPPs induce oxidative stress in ECs. Specificity of the dihydroethidium (DHE)-based probe for measurement of superoxide production was validated using ROS inhibitor YCG063 (Supplemental Methods and Figure S5). Next, we quantified peroxynitrite radical ($ONOO^-$) formation by staining HUVECs exposed to secondary CPPs for 24 hours for nitrotyrosine protein residues (3NT). A significant increase in 3NT-residues could be observed in ECs after CPP exposure (Figure 3D and 3E). This increase in protein damage was found in HUVECs stimulated with 50 and 100 µg/mL secondary CPPs for 24 hours. When staining the RCA rings (exposed to CPPs 0–400 µg/mL) for peroxynitrite radical formation, no clear differences could be observed in mean fluorescent 3NT pixel intensity (data not shown).

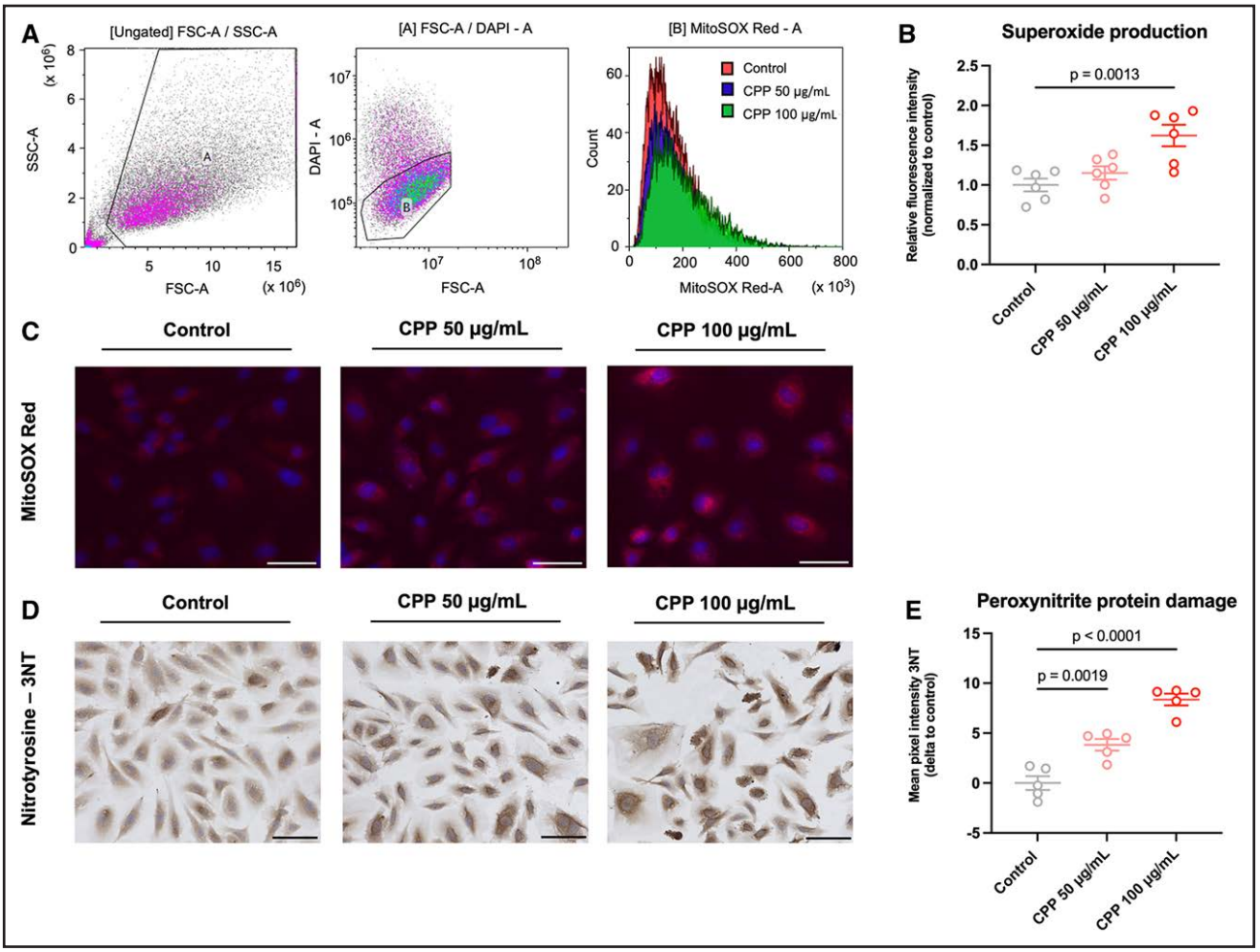

Figure 3. Secondary calciprotein particles (CPPs) induce superoxide formation and peroxynitrite radicals in endothelial cells. **A**, Flow cytometric analysis of superoxide generation (using the MitoSOX Red reagent) in endothelial cells exposed to secondary CPPs for 24 hours. **B**, Flow cytometric analysis showing a significant increase in superoxide formation in endothelial cells exposed to secondary CPPs (100 µg/mL) for 24 hours (DAPI positive cells excluded). **C**, Immunofluorescent MitoSOX Red staining showing increased superoxide levels in HUVECs exposed to secondary CPPs (50 and 100 µg/mL) for 24 hours. **D**, Immunohistochemical nitrotyrosine (3NT) protein staining of human umbilical vein endothelial cells (HUVECs) exposed to secondary CPPs (50 and 100 µg/mL) for 24 hours. **E**, Quantification of the 3NT protein staining showed that exposure of HUVECs to secondary CPPs for 24 hours induces a significant up regulation of nitrotyrosine protein residues. Data are normalized or show differences (Δ) to the experimental control. Graphs present means±SEM and individual data points. Significant differences are indicated for $P<0.05$. Scale bars represent 50 µm.

Calcification Propensity (OD_{650}) Associates With Renal Function and NO_x Levels

To translate our preclinical findings to a clinical setting, we collected serum samples within an early CKD patient cohort (n=245). Patients were divided based on calcification propensity (tertiles; low (n=81), medium (n=82) or high (n=82) OD_{650} increment), and baseline characteristics were measured (Table 1). Whereas total phosphate and Fetuin-A did not differ between the groups, total calcium, total protein and albumin levels were significantly lower in patients with a higher calcification propensity (all $P<0.01$). eGFR values were significantly lower in the medium and high OD_{650} increment tertiles, compared with the lowest OD_{650} increment tertile (Figure S6). CPP count did not differ between the tertiles (data not shown). Both OD_{650} increment (r=–0.217, $P<0.001$), and NO_x (ie, estimate for NO bioavailability; r=0.455, $P<0.001$) were significantly associated with the estimated glomerular filtration rate (eGFR; Figure 4A and 4B). Multivariable linear regression analyses, adjusting for demographics, smocking, body habitus, co-morbidity and mediation use, revealed that both OD_{650} (final model $P=0.040$) and NO_x (final model $P<0.001$) were robustly associated with eGFR (Table S2). Moreover, a significant association was found between calcification propensity and NO_x (r=–0.136; $P=0.049$; Figure 4C), indicating that an increase in secondary CPP formation could negatively influence NO bioavailability.

DISCUSSION

Accelerated formation and ripening of secondary CPPs is associated with the development of VCs and progression

Table 1. Baseline Demographic and Clinical Characteristics of an Early CKD Cohort

	Low OD_{650} increment (n=81)	Medium OD_{650} increment (n=82)	High OD_{650} increment (n=82)	*P* Value
Sex				0.773
Male	51 (63.0%)	56 (68.3%)	54 (65.9%)	
Female	30 (37.0%)	26 (31.7%)	28 (34.1%)	
Age, y*	62.4 (7.6)	63.2 (8.4)	64.9 (8.7)	0.128
eGFR, ml/min/1.73m²†	91.00 (80.50-99.00)‡	81.00 (66.00-95.00)	74.50 (64.75-90.00)	<0.001
Smoking	22 (27.2%)	30 (36.6%)	16 (19.5%)§	0.050
BMI, kg/m²†	28.70 (25.30-32.40)	27.85 (24.25-32.40)	27.45 (24.80-32.10)	0.525
OD_{650} increment†	0.003 (-0.005-0.007)	0.016 (0.013-0.020)	0.041 (0.029-0.056)	<0.001‖
NO_x, µmol/L†	4.63 (3.71-5.03)	3.90 (3.65-4.53)¶	4.04 (3.73-4.62)	0.003
Total calcium, mmol/L†	2.20 (2.05-2.30)‡	2.05 (1.92-2.24)	2.05 (1.89-2.27)	0.002
Ionised calcium, mmol/L†	0.90 (0.83-0.95)	0.96 (0.90-1.02)#	0.91 (0.86-0.98)	0.004
Total phosphate, mmol/L†	1.08 (0.95-1.20)	1.10 (0.96-1.24)	1.06 (0.94-1.21)	0.760
Total protein, g/L*	66.7 (8.4)‡	61.4 (8.5)	60.6 (8.4)	<0.001
Albumin, g/L*	39.4 (4.9)‡	37.1 (4.4)	36.0 (4.8)	<0.001
Fetuin-A, g/L†	0.30 (0.25-0.35)	0.31 (0.25-0.36)	0.30 (0.21-0.38)	0.880
Comorbidities				
Diabetes type 2	14 (17.3%)	14 (17.1%)	16 (19.5%)	0.903
COPD or Asthma	5 (6.2%)	11 (13.4%)	9 (11.0%)	0.299
Hypertension	53 (65.4%)	60 (73.2%)	62 (75.6%)	0.324
Chronic Heart Failure	31 (38.3%)	45 (54.9%)	53 (64.6%)¶	0.003
Medication				
Antiplatelets	32 (39.5%)	46 (56.1%)	41 (50.6%)	0.098
Beta-blockers	24 (29.6%)	35 (42.7%)	34 (42.0%)	0.156
ACE-inhibitors	21 (25.9%)	21 (25.6%)	16 (19.8%)	0.582
Statins	23 (28.4%)‡	49 (60.5%)	41 (50.6%)	<0.001
Nitrates	2 (2.5%)	21 (25.6%)#	8 (9.9%)	<0.001
Angiotensin blockers	18 (22.2%)	24 (29.3%)	18 (22.2%)	0.482
Aldosterone antagonist	4 (4.9%)	19 (23.2%)#	7 (8.8%)	0.001
Calcium-channel blockers	19 (23.5%)	25 (30.5%)	16 (19.8%)	0.270
Diuretics	6 (7.4%)	12 (14.6%)	8 (9.9%)	0.315
Anticoagulants	2 (2.5%)	7 (8.5%)	6 (7.4%)	0.231

Data are presented as numbers (n) with corresponding percentages (%; categorical variables) or as mean±SD (normal distribution) or median (interquartile range, 25–75; non-normal distribution; continuous variables). ACE indicates angiotensin-converting enzyme; BMI, body mass index; COPD, chronic obstructive pulmonary disorder; eGFR, estimated glomerular filtration rate; NO_x, sum of nitrate and nitrite; and OD_{650}, optical density increment at 650 nm wavelength.

*Normal distributed data are indicated with symbol.

†Not normal distributed data with symbol.

‡Significant difference with the second and third tertile.

§Significant difference with the first and second tertiles.

‖Significant across all pairwise comparisons.

¶Significant difference with the first tertile.

#Significant difference with the first and third tertile.

‡, §, ‖, ¶, #Significant differences after post-hoc testing with Bonferroni-adjustment for multiple comparisons.

of vascular diseases in patients with CKD.[11] Although the interaction between VSMCs and secondary CPPs during the development of VC has been extensively studied, the role of ECs in this process remains largely elusive. Here, we show for the first time that secondary CPPs hamper EC function by affecting the NO bioavailability and the NO metabolism. Generation of superoxides (O_2^-) is suggested to be a key factor in this process. Our clinical data support these findings by revealing a significant association between calcification propensity (OD_{650}) and NO_x levels. Taken together, our findings provide new evidence for direct effects of CPPs on ECs and pathways involved.

Primarily, we found that CPPs affect the EC-dependent relaxation of VSMCs by reducing the response to bradykinin, in a coronary artery ex vivo model. Bradykinin is a vasodilating substance, which can bind to the bradykinin B2 receptor on the cell surface of ECs.

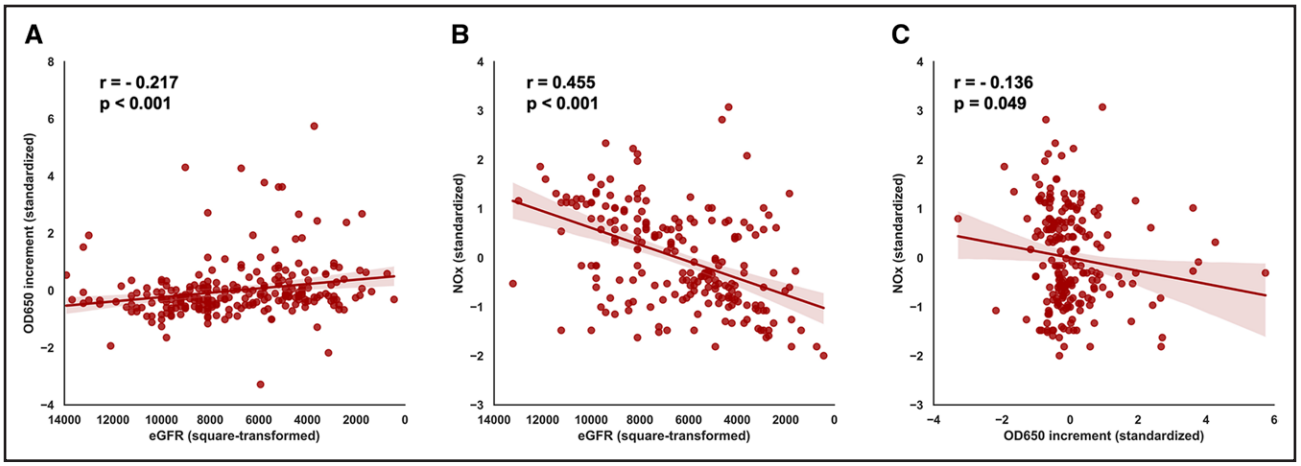

Figure 4. Scatterplots showing associations between calcification propensity (OD_{650}), NO_x, and estimated glomerular filtration rate (eGFR).

Associations were found between OD_{650} increment and eGFR (**A**, r=−0.217; *P*<0.001), NO_x, and eGFR (**B**, r=0.455, *P*<0.001) and NO_x and OD_{650} increment (**C**, r=−0.136; *P*=0.049). eGFR was square-transformed to achieve normally distributed distributions and homoscedasticity of residuals. Standardized (Z-transformed) OD_{650} and NO_x values are shown on the *y*-axes. Graphs show individual data points with a fitted regression line and 95% CI (color-shaded areas).

Receptor binding of bradykinin to ECs causes a rapid rise in calcium concentration and activates calmodulin and eNOS, leading to release of NO and relaxation of the VSMCs.[18,47] The reduced bradykinin-induced relaxation of ECs, observed in the ex vivo model, implies that CPPs alter the NO metabolism of ECs which deteriorates the VSMC relaxation. To unravel the underlying mechanisms, we performed several in vitro experiments in which ECs were exposed to different concentrations of CPPs and showed that CPPs decrease the NO bioavailability in ECs as demonstrated by decreased nitrite production, a frequently used biomarker for NO levels. Moreover, ECs showed a reduced eNOS expression and an increased eNOS protein uncoupling, expressed as a rise in monomer dissociation. Here, CPP-induced eNOS dysfunction, together with the reduced NO bioavailability, seem to be important triggers for the deteriorated EC-relaxation and EC dysfunction.

EC dysfunction is frequently associated with a reduced eNOS function in CKD.[31] For example, as a consequence of a decreased renal function in CKD, the uremic toxin asymmetric dimethylarginine can accumulate. Asymmetric dimethylarginine is an endogenous inhibitor of eNOS, which provokes eNOS uncoupling and subsequent endothelial cell and coronary dysfunction.[31,32,48] Likewise, advanced glycation end products (AGEs), including glycated proteins, lipids and nuclear acids, can accumulate in CKD and degrade eNOS mRNA, which is associated with the downregulation of the NO-synthase activity, and in the course of time leads to progression of arterial stiffness and atherosclerosis.[49,50] Shang et al[51] showed that when ECs in vitro are exposed to sera from CKD patients, miRNA-92a in the ECs becomes upregulated, which plays an important role in the inhibition of eNOS-mediated NO bioavailability. Additionally, we found that an increased calcification propensity (OD_{650}) is associated with reduced NO_x values in our early CKD cohort, indicating that an increment in secondary CPP formation could contribute to a decreased NO bioavailability. Although all these studies indicate circulating serum compounds as key triggers for eNOS dysfunction, and consequently a decreased NO bioavailability in CKD, an unanswered question remains, especially for the circulating secondary CPPs, how these particles initiate eNOS dysfunction and how this leads to EC impairment.

Previously, we have demonstrated that ECs internalize CPPs when visualizing the cells with transmission electron microscopy.[52] Internalization of the CPPs is accompanied by an influx of calcium ions in both lysosomes and cytosol.[53] These data suggest that active uptake of the particles from the circulating blood could lead to an intracellular calcium increase. Additionally, an intracellular calcium overload is associated with mitochondrial calcium buffering, and if not compensated, mitochondrial calcium buffering can lead to ROS formation.[54] We found a significant upregulation in superoxide (O_2^-) production in the ECs after CPP exposure, indicating oxidative stress. It is tempting to speculate that CPP uptake by ECs causes a mitochondrial calcium overload, which leads to superoxide generation, however, certainly more research is needed to confirm this hypothesis. On the other hand, cellular stress can also lead to O_2^- generation via, for example, NADPH oxidases.[23] Increased superoxide levels are detrimental for ECs because they can oxidize cofactors, like BH_4, which are required for normal eNOS functioning. In the absence of functional co-factors, eNOS becomes uncoupled and starts to produce superoxides as well, instead of NO.[19] Here, the negative feedback loop of O_2^- generation begins. We now extend these data and show that CPPs induce

eNOS uncoupling which may contribute to the ROS formation. Notably, a recent study of Chen et al[55] indicated that during eNOS uncoupling, phosphorylation of eNOS residue Ser1177 further promotes O_2^- production. In line with this, we also observed increased eNOS phosphorylation of residue Ser1177 in HUVECs after CPP exposure. Due to the increased superoxide levels in HUVECs, peroxynitrite radical ($ONOO^-$) formation was confirmed, marked by a rise in nitrotyrosine (3NT) protein residue formation. 3NT protein residue formation blunts protein activity (eg, eNOS) and it is not unlikely that peroxynitrite radical formation contributes to CPP-induced EC dysfunction.

Having discussed how CPPs could induce eNOS dysfunction, NO deficits and EC dysfunction, a final point to speculate about is how CPP-induced EC dysfunction could possibly enhance vascular calcification in CKD. A study by Oe et al recently showed that eNOS deficiency seems to play an important role in the progression of vascular calcification. eNOS deficient mice ($eNOS^{-/-}$) fed with an adenine high phosphate diet suffered a higher calcium deposition in the aorta, together with increased RUNX2 (runt-related transcription factor 2) expression and increased markers of oxidative stress compared with the wild-type mice.[56] NOS-derived NO is known as important anti-oxidant compound, which scavenges multiple forms of radicals.[56,57] As oxidative stress is an important contributor to the development of vascular calcification, this raises the question whether NO supplementation might by an important therapeutic target in the development of CPP-induced vascular calcification. In a study from De Meyer et al,[58] it was shown that NO supplementation, via NO-donor Molsidomine, significantly reduced superoxide production of atherosclerotic aortas and increased features of stabilized plaques, during cholesterol lowering in rabbits. Furthermore, a study from Guzik et al showed that incubation of human internal mammary arteries with NO-donor SNP significantly decreased superoxide production by the different artery segments, hinting anti-oxidant effects of NO. Nevertheless, the same study also demonstrated that the supplementation of SNP led to significantly increased peroxynitrite formation by the artery wall.[59] These data illustrate that although supplementation of NO can be beneficial as scavenger of oxidative stress, caution is warranted when considering NO-enhancing therapeutics, to prevent over-supplementation and promote the production of reactive nitrogen species like $ONOO^-$, which can have detrimental consequences.[59,60] Additionally, it is crucial to mention that research on CPP-induced vascular calcification is still in its infancy, and additional experiments are required to first of establish a clear link between CPP-induced endothelial dysfunction and the development of vascular calcification, and secondly to validate therapeutic targets for interfering or preventing this pathology.

A strength of the current study is the combined use of both experimental data (eg, in vitro and ex vivo) and clinical data to analyze, and translate, the effects of secondary CPPs on EC function. The inclusion of a large, well-characterized patient cohort revealed associations between calcification propensity and NO metabolism which supports our mechanistic in vitro finings. One should realize that associations as such do not necessarily imply causal relations and other aspects of the CKD milieu might be involved as well. Additionally, the inclusion of patients within the mild to moderate stages of CKD (stage 1–3), allowed us to study early onset of vascular damage due to an increased serum calcification propensity. Where most of the literature is focusing on calcification propensity and CPP formation within end-stage renal disease or renal transplant recipient,[10,61,62] insights in the early development of vascular damage is lacking. Here, our data obtained from the early CKD patient cohort are of added value.

Furthermore, very little is known about the actual physiological concentration of CPPs in CKD patients. As previously mentioned, serum T_{50} values (ie, transition time from primary to secondary CPPs) are lower in CKD patients compared with healthy controls.[12,61,62] Nevertheless, how T_{50} values relate to actual CPP concentrations is largely unknown. In the current study, we used in vitro and ex vivo CPP concentrations based on previous studies,[14,63,64] assuming that exposure time in vivo is a long-term process and this prompts adjustment of the CPP concentration to correct for the shorter exposure time in our experimental set-up, resulting in the use of slightly higher concentrations. Still, we would like to emphasize the need for future studies determining the true tissue exposure to CPPs. Studies as such will most likely increase the accuracy and reliability of CPP-based in vitro and ex vivo experiments and more closely mimic the in vivo situation.

With regard to the ex vivo porcine coronary artery rings, it can be considered whether the use of exclusively female porcine tissue affects the outcome of the experiments, since sex differences can influence the development of vascular diseases. Female ECs largely depend on eNOS functioning for EC-dependent relaxation, and alterations in eNOS function might therefore affect the response of VSMC relaxation.[65] In the interest of the dependence of eNOS function in female porcine tissue relaxation, we suggest that the use of exclusively female tissue in this study can be valuable, since it may show more abundantly the detrimental effects of CPPs on eNOS function, then when using only a male or mixed porcine tissue selection, wherein eNOS activity seem to be less required. For the in vitro experiments, we used a large human umbilical vein endothelial cell pool comprising both female and male donors to perform underlying pathway analysis. Likewise, clinical data analysis was performed in an early CKD cohort with both sexes.

In conclusion, our findings demonstrate for the first time that secondary CPPs cause EC dysfunction by impairing the NO metabolism. These insights provide further understanding of the interaction between CPPs and ECs, but more importantly propose ECs as a novel target for intervention.

ARTICLE INFORMATION

Received April 25, 2022; accepted January 18, 2023.

Affiliations

Department of Pathology and Medical Biology (L.F., G.K., J.-L.H.), Department of Clinical Pharmacy and Pharmacology (H.B., G.K.), and Department of Gastroenterology and Hepatology (A.R.B.), University of Groningen, University Medical Center Groningen, The Netherlands. Laboratory for Molecular, Translational and Digital Medicine, Research Institute for Complex Issues of Cardiovascular Diseases, Kemerovo, Russian Federation (A.G.K., D.K.S.). Department of Physiology, Radboud Institute for Molecular Life Sciences, Radboud University Medical Center, Nijmegen, The Netherlands (L.W.Z.).

Acknowledgments

The authors thank the endothelial cell facility of the Medical Biology Department, University Medical Center Groningen, Groningen, the Netherlands for providing the HUVECs for this paper. Additionally, we would like to thank Anja Bakker, Mirjam Mastik, Monique Lodewijk, Geert Mesander, Linda Brouwer, Azuwerus van Buiten, and Victoria E. Markova for their technical support during the experiments, and Anton J.M. Roks for his contribution to the content and discussion of the article. The graphical abstract was created with BioRender.com.

Sources of Funding

Financial support for this study was provided to L. Feenstra by the Graduated School of Medical Sciences of the University of Groningen, the Netherlands (in vitro and ex vivo experiments). A.G. Kutikhin and D.K. Shishkova were supported by the Russian Science Foundation (grant 22-15-00107 [Circulation of calciprotein particles in human blood: pathogenic consequences and molecular mechanisms], clinical study). A.R. Bourgonje is supported by the M.D.- Ph.D. trajectory grant (17-57) from the Junior Scientific Masterclass (JSM) of the University of Groningen, the Netherlands. J.-L. Hillebrands is principle investigator in NIGRAM2+ (NIer Gerichte Research van Arterie tot Mens: centrale rol voor Magnesium ++) consortium, funded by Health Holland (LSHM17034) and the Dutch Kidney Foundation (16TKI02). L.W. Zeper received financial support from Health Holland (LSHM17034) and the Dutch Kidney Foundation (16TKI02), within the NIGRAM2+ consortium.

Disclosures

G. Krenning is Chief Officer of Sulfateq B.V. (Groningen, the Netherlands), a company that develops small molecule therapeutics. Sulfateq B.V. has no small molecule in development for anti-circulating calciprotein particle (CPP) therapy at present and had no influence on the content of this article. The other authors report no conflict of interest.

Supplemental Material

Supplemental Methods
Figure S1–S8
Tables S1 and S2
Major Resources Table

REFERENCES

1. Jankowski J, Floege J, Fliser D, Böhm M, Marx N. Cardiovascular disease in chronic kidney disease. *Circulation*. 2021;143:1157–1172. doi: 10.1161/circulationaha.120.050686
2. Disthabanchong S. Vascular calcification in chronic kidney disease: pathogenesis and clinical implication. *World J Nephrol*. 2012;1:43–53. doi: 10.5527/wjn.v1.i2.43
3. Paloian NJ, Giachelli CM. A current understanding of vascular calcification in CKD. *Am J Physiol Renal Physiol*. 2014;307:F891891–F89F900. doi: 10.1152/ajprenal.00163.2014
4. Moe SM, Chen NX. Mechanisms of vascular calcification in chronic kidney disease. *J Am Soc Nephrol*. 2008;19:213–216. doi: 10.1681/ASN.2007080854
5. Sedaghat S, Hoorn EJ, Ikram MA, Koop-Nieuwelink C, Kavousi M, Franco OH, van der Lugt A, Vernooij MW, Bos D. Kidney function and arterial calcification in major vascular beds. *J Am Heart Assoc*. 2019;8:e010930. doi: 10.1161/JAHA.118.010930
6. Holt SG, Smith ER. Fetuin-A-containing calciprotein particles in mineral trafficking and vascular disease. *Nephrol Dial Transplant*. 2016;31:1583–1587. doi: 10.1093/ndt/gfw048
7. Schlieper G, Schurgers L, Brandenburg V, Reutelingsperger C, Floege J. Vascular calcification in chronic kidney disease: an update. *Nephrol Dial Transplant*. 2016;31:31–39. doi: 10.1093/ndt/gfv111
8. Pasch A, Farese S, Gräber S, Wald J, Richtering W, Floege J, Jahnen-Dechent W. Nanoparticle-based test measures overall propensity for calcification in serum. *J Am Soc Nephrol*. 2012;23:1744–1752. doi: 10.1681/asn.2012030240
9. Köppert S, Büscher A, Babler A, Ghallab A, Buhl EM, Latz E, Hengstler JG, Smith ER, Jahnen-Dechent W. Cellular clearance and biological activity of calciprotein particles depend on their maturation state and crystallinity. *Front Immunol*. 2018;9:1991. doi: 10.3389/fimmu.2018.01991
10. Smith ER, Ford ML, Tomlinson LA, Bodenham E, McMahon LP, Farese S, Rajkumar C, Holt SG, Pasch A. Serum calcification propensity predicts all-cause mortality in predialysis CKD. *J Am Soc Nephrol*. 2014;25:339–348. doi: 10.1681/ASN.2013060635
11. Kutikhin AG, Feenstra L, Kostyunin AE, Yuzhalin AE, Hillebrands JL, Krenning G. Calciprotein particles. *Arterioscler Thromb Vasc Biol*. 2021;41:1607–1624. doi: 10.1161/atvbaha.120.315697
12. Bundy JD, Cai X, Mehta RC, Scialla JJ, de Boer IH, Hsu C-yuan, Go AS, Dobre MA, Chen J, Rao PS, et al. Serum calcification propensity and clinical events in CKD. *Clin J Am Soc Nephrol*. 2019;14:1562–1571. doi: 10.2215/cjn.04710419
13. Smith ER, Ford ML, Tomlinson LA, Rajkumar C, McMahon LP, Holt SG. Phosphorylated fetuin-A-containing calciprotein particles are associated with aortic stiffness and a procalcific milieu in patients with pre-dialysis CKD. *Nephrol Dial Transplant*. 2012;27:1957–1966. doi: 10.1093/ndt/gfr609
14. Aghagolzadeh P, Bachtler M, Bijarnia R, Jackson C, Smith ER, Odermatt A, Radpour R, Pasch A. Calcification of vascular smooth muscle cells is induced by secondary calciprotein particles and enhanced by tumor necrosis factor-α. *Atherosclerosis*. 2016;251:404–414. doi: 10.1016/j.atherosclerosis.2016.05.044
15. Viegas CSB, Santos L, Macedo AL, Matos AA, Silva AP, Neves PL, Staes A, Gevaert K, Morais R, Vermeer C, et al. Chronic kidney disease circulating calciprotein particles and extracellular vesicles promote vascular calcification. *Arterioscler Thromb Vasc Biol*. 2018;38:575–587. doi: 10.1161/ATVBAHA.117.310578
16. Krüger-Genge A, Blocki A, Franke RP, Jung F. Vascular endothelial cell biology: an update. *Int J Mol Sci* . 2019;20:4411. doi: 10.3390/ijms20184411
17. Durand MJ, Gutterman DD. Diversity in mechanisms of endothelium-dependent vasodilation in health and disease. *Microcirculation*. 2013;20:239–247. doi: 10.1111/micc.12040
18. Zhao Y, Vanhoutte PM, Leung SWS. Vascular nitric oxide: beyond eNOS. *J Pharmacol Sci*. 2015;129:83–94. doi: 10.1016/j.jphs.2015.09.002
19. Förstermann U, Sessa WC. Nitric oxide synthases: regulation and function. *Eur Heart J*. 2012;33:829–837. doi: 10.1093/eurheartj/ehr304
20. Sessa WC. eNOS at a glance. *J Cell Sci*. 2004;117:2427–2429. doi: 10.1242/jcs.01165
21. Davignon J, Ganz P. Role of endothelial dysfunction in atherosclerosis. *Circulation*. 2004;109:27–32. doi: 10.1161/01.CIR.0000131515.03336.f8
22. Hermann M, Flammer A, Lüscher TF. Nitric oxide in hypertension. *The Journal of Clinical Hypertension*. 2006;8:17–29. doi: 10.1111/j.1524-6175.2006.06032.x
23. Takabe W, Jen N, Ai L, Hamilton R, Wang S, Holmes K, Dharbandi F, Khalsa B, Bressler S, Barr ML, et al. Oscillatory shear stress induces mitochondrial superoxide production: implication of NADPH oxidase and c-Jun NH 2 -terminal kinase signaling. *Antioxid Redox Signal*. 2011;15:1379–1388. doi: 10.1089/ars.2010.3645
24. Quijano C, Castro L, Peluffo G, Valez V, Radi R. Enhanced mitochondrial superoxide in hyperglycemic endothelial cells: direct measurements and formation of hydrogen peroxide and peroxynitrite. *Am J Physiol Heart Circ Physiol*. 2007;293:H34043404–H340H3414. doi: 10.1152/ajpheart.00761.2007
25. Patel H, Chen J, Das KC, Kavdia M. Hyperglycemia induces differential change in oxidative stress at gene expression and functional levels in HUVEC and HMVEC. *Cardiovasc Diabetol*. 2013;12:142. doi: 10.1186/1475-2840-12-142
26. Martens CR, Edwards DG. Peripheral vascular dysfunction in chronic kidney disease. *Cardiol Res Pract*. 2011;2011:1–9. doi: 10.4061/2011/267257

27. Li H, Förstermann U. Uncoupling of endothelial NO synthase in atherosclerosis and vascular disease. *Curr Opin Pharmacol*. 2013;13:161–167. doi: 10.1016/j.coph.2013.01.006
28. Łuczak A, Madej M, Kasprzyk A, Doroszko A. Role of the eNOS uncoupling and the nitric oxide metabolic pathway in the pathogenesis of autoimmune rheumatic diseases. *Oxid Med Cell Longev*. 2020;2020:1–15. doi: 10.1155/2020/1417981
29. Arunachalam G, Samuel SM, Ding H, Triggle CR. Peroxynitrite biology. In: Laher I, ed. *Systems Biology of Free Radicals and Antioxidants*. Springer Berlin Heidelberg; 2014:207–242.
30. Pacher P, Beckman JS, Liaudet L. Nitric oxide and peroxynitrite in health and disease. *Physiol Rev*. 2007;87:315–424. doi: 10.1152/physrev.00029.2006
31. Roumeliotis S, Mallamaci F, Zoccali C. Endothelial dysfunction in chronic kidney disease, from biology to clinical outcomes: a 2020 update. *J Clin Med*. 2020;9:2359. doi: 10.3390/jcm9082359
32. Tatematsu S, Wakino S, Kanda T, Homma K, Yoshioka K, Hasegawa K, Sugano N, Kimoto M, Saruta T, Hayashi K. Role of nitric oxide–producing and –degrading pathways in coronary endothelial dysfunction in chronic kidney disease. *J Am Soc Nephrol*. 2007;18:741–749. doi: 10.1681/asn.2006040367
33. Echeverry-Rendón M, Echeverria F, Buikema H, Harmsen MC, Krenning G. Endothelial function after the exposition of magnesium degradation products. *Biomaterials Advances*. 2022;134:112693. doi: 10.1016/j.msec.2022.112693
34. Buikema H, Grandjean JG, van den Broek S, van Gilst WH, Lie KI, Wesseling H. Differences in vasomotor control between human gastroepiploic and left internal mammary artery. *Circulation*. 1992;86:205–209.
35. Zeebregts C, van den Dungen J, Buikema H, Tiebosch A, van der Want J, van Schilfgaarde R. Preservation of endothelial integrity and function in experimental vascular anastomosis with non-penetrating clips. *Br J Surg*. 2002;88:1201–1208. doi: 10.1046/j.0007-1323.2001.01857.x
36. Gschwend S, Pinto-Sietsma SJ, Buikema H, Pinto YM, Van Gilst WH, Schulz A, De Zeeuw D, Kreutz R. Impaired coronary endothelial function in a rat model of spontaneous albuminuria. *Kidney Int*. 2002;62:181–191. doi: 10.1046/j.1523-1755.2002.00431.x
37. Myers PR, Banitt PF, Guerra R, Harrison DG. Role of the endothelium in modulation of the acetylcholine vasoconstrictor response in porcine coronary microvessels. *Cardiovasc Res*. 1991;25:129–137. doi: 10.1093/cvr/25.2.129
38. Zhou Y, Varadharaj S, Zhao X, Parinandi N, Flavahan NA, Zweier JL. Acetylcholine causes endothelium-dependent contraction of mouse arteries. *Am J Physiol Heart Circ Physiol*. 2005;289:H10271027–H102H1032. doi: 10.1152/ajpheart.00226.2005
39. Grover AK, Samson SE, Misquitta CM, Elmoselhi AB. Effects of peroxide on contractility of coronary artery rings of different sizes. *Mol Cell Biochem*. 1999;194:159–164. doi: 10.1023/a:1006902603056
40. Burgess WH, Mehlman T, Friesel R, Johnson W, Maciag T. Multiple forms of endothelial cell growth factor. Rapid isolation and biological and chemical characterization. *J Biol Chem*. 1985;260:11389–11392. doi: 10.1016/s0021-9258(17)39038-5
41. Shiva SN. A physiological store of nitric oxide and modulator of mitochondrial function. *Redox Biol*. 2013;1:40–44. doi: 10.1016/j.redox.2012.11.005
42. Schneider CA, Rasband WS, Eliceiri KW. NIH Image to ImageJ: 25 years of image analysis. *Nat Methods*. 2012;9:671–675. doi: 10.1038/nmeth.2089
43. Oberhuber R, Riede G, Cardini B, Bernhard D, Messner B, Watschinger K, Steger C, Brandacher G, Pratschke J, Golderer G, et al. Impaired endothelial nitric oxide synthase homodimer formation triggers development of transplant vasculopathy - insights from a murine aortic transplantation model. *Sci Rep*. 2016;6:37917. doi: 10.1038/srep37917
44. Gumanova NG, Deev AD, Kots AY, Shalnova SA. Elevated levels of serum nitrite and nitrate, NOx, are associated with increased total and cardiovascular mortality in an 8-year follow-up study. *Eur J Clin Invest*. 2018;49:e13061. doi: 10.1111/eci.13061
45. Smith ER, Hewitson TD, Cai MMX, Aghagolzadeh P, Bachtler M, Pasch A, Holt SG. A novel fluorescent probe-based flow cytometric assay for mineral-containing nanoparticles in serum. *Sci Rep*. 2017;7:5686. doi: 10.1038/s41598-017-05474-y
46. Caligiuri G. CD31 as a therapeutic target in atherosclerosis. *Circ Res*. 2020;126:1178–1189. doi: 10.1161/circresaha.120.315935
47. Bae SW, Kim HS, Cha YN, Park YS, Jo SA, Jo I. Rapid increase in endothelial nitric oxide production by bradykinin is mediated by protein kinase A signaling pathway. *Biochem Biophys Res Commun*. 2003;306:981–987. doi: 10.1016/s0006-291x(03)01086-6
48. Vallance P, Leone A, Calver A, Collier J, Moncada S. Accumulation of an endogenous inhibitor of nitric oxide synthesis in chronic renal failure. *Lancet*. 1992;339:572–575. doi: 10.1016/0140-6736(92)90865-z
49. Cuenca MV, Hordijk PL, Vervloet MG. Most exposed: the endothelium in chronic kidney disease. *Nephrol Dial Transplant*. 2020;35:1478–1487. doi: 10.1093/ndt/gfz055
50. Stinghen AEM, Massy ZA, Vlassara H, Striker GE, Boullier A. Uremic toxicity of advanced glycation end products in CKD. *J Am Soc Nephrol*. 2016;27:354–370. doi: 10.1681/ASN.2014101047
51. Shang F, Wang SC, Hsu CY, Miao Y, Martin M, Yin Y, Wu C-C, Wang Y-T, Wu G, Chien S, et al. MicroRNA-92a mediates endothelial dysfunction in CKD. *J Am Soc Nephrol*. 2017;28:3251–3261. doi: 10.1681/asn.2016111215
52. Kutikhin AG, Velikanova EA, Mukhamadiyarov RA, Glushkova TV, Borisov VV, Matveeva VG, Antonova LV, Filip'ev DE, Golovkin AS, Shishkova DK, et al. Apoptosis-mediated endothelial toxicity but not direct calcification or functional changes in anti-calcification proteins defines pathogenic effects of calcium phosphate bions. *Sci Rep*. 2016;6:27255. doi: 10.1038/srep27255
53. Shishkova DK, Velikanova EA, Bogdanov LA, Sinitsky MY, Kostyunin AE, Tsepokina AV, Gruzdeva OV, Mironov AV, Mukhamadiyarov RA, Glushkova TV, et al. Calciprotein particles link disturbed mineral homeostasis with cardiovascular disease by causing endothelial dysfunction and vascular inflammation. *Int J Mol Sci* . 2021;22:12458. doi: 10.3390/ijms222212458
54. Brookes PS, Yoon Y, Robotham JL, Anders MW, Sheu SS. Calcium, ATP, and ROS: a mitochondrial love-hate triangle. *Am J Physiol Cell Physiol*. 2004;287:C817817–C81C833. doi: 10.1152/ajpcell.00139.2004
55. Chen CA, Druhan LJ, Varadharaj S, Chen YR, Zweier JL. Phosphorylation of endothelial nitric-oxide synthase regulates superoxide generation from the enzyme. *J Biol Chem*. 2008;283:27038–27047. doi: 10.1074/jbc.m802269200
56. Oe Y, Mitsui S, Sato E, Shibata N, Kisu K, Sekimoto A, Miyazaki M, Sato H, Ito S, Takahashi N. Lack of endothelial nitric oxide synthase accelerates ectopic calcification in uremic mice fed an adenine and high phosphorus diet. *Am J Pathol*. 2021;191:283–293. doi: 10.1016/j.ajpath.2020.10.012
57. Kanner J, Harel S, Rina G. Nitric oxide as an antioxidant. *Arch Biochem Biophys*. 1991;289:130–136. doi: 10.1016/0003-9861(91)90452-o
58. de Meyer GRY, Kockx MM, Knaapen MWM, Martinet W, De Cleen DM, Bult H, Herman AG. Nitric oxide donor molsidomine favors features of atherosclerotic plaque stability during cholesterol lowering in rabbits. *J Cardiovasc Pharmacol*. 2003;41:970–978. doi: 10.1097/00005344-200306000-00021
59. Guzik TJ, West NEJ, Pillai R, Taggart DP, Channon KM. Nitric oxide modulates superoxide release and peroxynitrite formation in human blood vessels. *Hypertension*. 2002;39:1088–1094. doi: 10.1161/01.HYP.0000018041.48432.B5
60. Herman AG, Moncada S. Therapeutic potential of nitric oxide donors in the prevention and treatment of atherosclerosis. *Eur Heart J*. 2005;26:1945–1955. doi: 10.1093/eurheartj/ehi333
61. Keyzer CA, de Borst MH, van den Berg E, Jahnen-Dechent W, Arampatzis S, Farese S, Bergmann IP, Floege J, Navis G, Bakker SJL, et al. Calcification propensity and survival among renal transplant recipients. *J Am Soc Nephrol*. 2016;27:239–248. doi: 10.1681/ASN.2014070670
62. Dahle DO, Åsberg A, Hartmann A, Holdaas H, Bachtler M, Jenssen TG, Dionisi M, Pasch A. Serum calcification propensity is a strong and independent determinant of cardiac and all-cause mortality in kidney transplant recipients. *Am J Transplant*. 2016;16:204–212. doi: 10.1111/ajt.13443
63. Smith ER, Hanssen E, McMahon LP, Holt SG. Fetuin-A-containing calciprotein particles reduce mineral stress in the macrophage. Ojcius DM, ed. *PLoS One*. 2013;8:e60904. doi: 10.1371/journal.pone.0060904
64. ter Braake AD, Eelderink C, Zeper LW, Pasch A, Bakker SJL, de Borst MH, Hoenderop JGJ, de Baaij JHF. Calciprotein particle inhibition explains magnesium-mediated protection against vascular calcification. *Nephrol Dial Transplant*. 2020;35:765–773. doi: 10.1093/ndt/gfz190
65. Cattaneo MG, Vanetti C, Decimo I, Di Chio M, Martano G, Garrone G, Bifari F, Vicentini LM. Sex-specific eNOS activity and function in human endothelial cells. *Sci Rep*. 2017;7:9612. doi: 10.1038/s41598-017-10139-x